INTERNATIONAL JOURNAL OF HYDROGEN ENERGY XXX (2015) 1–8

Available online at www.sciencedirect.com

ScienceDirect

journal homepage: www.elsevier.com/locate/he

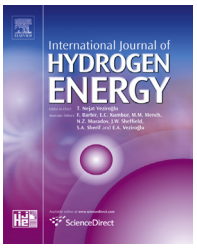

$Sr_2Fe_{1+x}Mo_{1-x}O_{6-\delta}$ as anode material of cathode–supported solid oxide fuel cells

*Guoshuan Miao, Chun Yuan, Ting Chen, Yucun Zhou, Weiting Zhan, Shaorong Wang**

CAS Key Laboratory of Materials for Energy Conversion, Shanghai Institute of Ceramics, Chinese Academy of Sciences (SICCAS), 1295 Ding-xi Road, Shanghai 200050, China

ARTICLE INFO

Article history:
Received 4 July 2015
Received in revised form
2 December 2015
Accepted 13 December 2015
Available online xxx

Keywords:
Molybdenum doped strontium ferrite
Anode
Cathode–supported
Solid oxide fuel cell

ABSTRACT

In this study, perovskite-type oxides of $Sr_2Fe_{1+x}Mo_{1-x}O_{6-\delta}$ (x = 0, 0.2, 0.35, 0.5) were synthesized and the phase stabilities both in oxidizing and reducing atmosphere were investigated. When calcined in the air atmosphere, pure perovskite phase can be obtained for the composition of $Sr_2Fe_{1.5}Mo_{0.5}O_{6-\delta}$ while a large portion of $SrMoO_4$ second phase was detected in other compositions. Further reducing the above powders showed a pure phase for $Sr_2Fe_{1+x}Mo_{1-x}O_{6-\delta}$ (x = 0, 0.2, 0.35) while minor amount of Fe was precipitated from the $Sr_2Fe_{1.5}Mo_{0.5}O_{6-\delta}$. Due to the highest electrical conductivity and lowest polarization resistance of $Sr_2FeMoO_{6-\delta}$, such composition has been applied as the cell anode for a cathode supported solid oxide fuel cell (CS-SOFC). Maximum power densities of 463 and 331 mW cm^{-2} have obtained for the fuel cell when measured at 800 °C using hydrogen and propane as fuel, respectively. The durability test in propane indicated that $Sr_2FeMoO_{6-\delta}$ could be a potential anode material with good tolerance ability toward coking formation.
Copyright © 2015, Hydrogen Energy Publications, LLC. Published by Elsevier Ltd. All rights reserved.

Introduction

Solid Oxide Fuel Cells (SOFCs) can directly convert the chemical energy of fuels like hydrogen, natural gas and propane into electricity in a highly efficient and environmental friendly way [1]. The high operation temperature of SOFC facilitates the utilization of low cost hydrocarbon fuels [2–6]. Nickel/yttria-stabilized zirconia (Ni/YSZ) cermet has been widely used as an excellent anode material due to its high catalytic activity toward hydrogen oxidation [7]. However, when hydrocarbon fuels are directly fed into Ni/YSZ anode, the nickel particles tend to catalyze the carbon deposition, resulting in quick performance degradation of the cells [8]. In order to solve this issue, many perovskite materials such as $La_xSr_{1-x}TiO_3$(LST) [9], $La_{0.75}Sr_{0.25}Cr_{0.5}Mn_{0.5}O_{3-\delta}$ (LSCM) [10], $La_{0.75}Sr_{0.25}Cr_{0.5}Fe_{0.5}O_{3-\delta}$ [11] and $SrMMoO_{6-\delta}$ (M = Mg, Co, Ni) [12–14] have been investigated as potential anode materials.

In recent years, $Sr_2Fe_{1.5}Mo_{0.5}O_{6-\delta}$ (SFMO) has gradually become the hotspot in the research of both cathode [15–17] and anode materials [18–20]. SFMO has a perovskite structure and could be stable in a wide temperature range in both reducing and oxiding atmosphere [21]. This material shows the characteristic of mixed ionic and electronic conductivity due to the hybridization of $Fe^{2+}/Mo^{6+}$and Fe^{3+}/Mo^{5+} [22]. When measured in oxidizing atmosphere, the ionic conductivity of SFMO is higher than that of the traditional $La_{0.8}Sr_{0.2}MnO_3$ and is even comparable to that of the

* *Corresponding author*. Tel.: +86 21 6990 6382; fax: +86 21 5241 3903.
E-mail address: miaoguoshuan@student.sic.ac.cn (S. Wang).
http://dx.doi.org/10.1016/j.ijhydene.2015.12.045
0360-3199/Copyright © 2015, Hydrogen Energy Publications, LLC. Published by Elsevier Ltd. All rights reserved.

Please cite this article in press as: Miao G, et al., $Sr_2Fe_{1+x}Mo_{1-x}O_{6-\delta}$ as anode material of cathode–supported solid oxide fuel cells, International Journal of Hydrogen Energy (2015), http://dx.doi.org/10.1016/j.ijhydene.2015.12.045

$La_{0.6}Sr_{0.4}Co_{0.2}Fe_{0.8}O_3$ [23]. Meanwhile, SFMO exhibits comparable electronic conductivity to the conventional nickel-cermet anode when measured in reducing atmosphere [22]. Furthermore, SFMO has also shown good anti-carbon deposition effects. A direct methanol SOFC all perovskite showed a power density of 391 mW cm^{-2} at 800 °C and no carbon formation was found in the cell's anode after operating in methanol [24]. Wang et al. also reported a SOFC with $Sr_2FeMoO_{6-\delta}$ anode which exhibited a power density of 604.8 mW cm^{-2} in CH_4 at 850 °C [25]. The durability test demonstrated that the stability of the cells with $Sr_2FeMoO_{6-\delta}$ anode was much better than with Ni based anodes when operated in dry CH_4. In addition, $Sr_2Fe_{1.33}Mo_{0.67}O_{6-\delta}$ have also been studied as the anodes for SOFCs with anti-carbon deposition ability [26]. Although all these reports indicated that $Sr_2Fe_{1+x}Mo_{1-x}O_{6-\delta}$ with different composition have good carbon resistance and excellent catalytic activity for the oxidation of the hydrocarbon fuels, the influence of the ratio of Fe: Mo on the anode performance has not been comparatively well studied.

In this paper, the phase stability of $Sr_2Fe_{1+x}Mo_{1-x}O_{6-\delta}$ (x = 0, 0.2, 0.35, 0.5) series materials in both oxidizing and reducing atmosphere is studied. With the main interest in anode, the conductivity in reducing atmosphere and electrochemical performances of SOFCs with the impregnated $Sr_2Fe_{1+x}Mo_{1-x}O_{6-\delta}$ anodes are also investigated.

Experimental

Powder preparation

$Sr_2Fe_{1+x}Mo_{1-x}O_{6-\delta}$ (x = 0, 0.2, 0.35, 0.5) powders were synthesized by a combined EDTA and citric acid complexing method with $Sr(NO_3)_2$, $Fe(NO_3)_3{\cdot}9H_2O$, $(NH_4)_6Mo_7O_{24}{\cdot}4H_2O$ as the raw materials [25]. All the starting chemicals were of analytical grade and purchased from Sinopharm Chemical Reagent Co., Ltd. EDTA was added into the aqueous ammonia to form a homogenous solution, followed by dissolving a certain amount of $(NH_4)_6Mo_7O_{24}{\cdot}4H_2O$ while heating and stirring. The stoichiometric amounts of $Sr(NO_3)_2$, $Fe(NO_3)_3{\cdot}9H_2O$ were first dissolved into the deionized water and then added into the EDTA-$NH_3{\cdot}H_2O$ solution. After stirring, proper amount of citric acid was introduced. The mole ratio of EDTA:citrate:total metal ions was controlled to be 2:2:1. The pH value of the solution was adjusted to about 8 *via* the addition of $NH_3{\cdot}H_2O$. The solution was then dried and calcined at 850–1100 °C in air for 2–5 h to form the desired $Sr_2Fe_{1+x}Mo_{1-x}O_{6-\delta}$ phase. The obtained $Sr_2Fe_{1+x}Mo_{1-x}O_{6-\delta}$ powders were further reduced in 97% H_2–3% H_2O at 800 °C for 2–20 h.

Single cell fabrication

The scaffold of cathode-supported SOFC ($(La_{0.8}Sr_{0.2})_{0.95}MnO_3$ (LSM) support/porous 8 mol% Y_2O_3-stabilized ZrO_2 (YSZ)/YSZ/porous YSZ) was fabricated by laminating four tape-casted green tapes under a pressure of 3000 psi at 75 °C for 10 min [27]. The laminated green tapes were then co-sintered at 1250 °C for 4 h in air [28]. Wet chemical impregnation was introduced to build the active catalysts for both the cathode and the anode. The cathode catalyst $La_{0.6}Sr_{0.4}Fe_{0.9}Sc_{0.1}O_{3-\delta}$ (LSFSc) was introduced into the porous YSZ backbone (close to LSM support layer) by impregnating nitrate solution containing $La(NO_3)_3{\cdot}6H_2O$, $Sr(NO_3)_2$, $Fe(NO_3)_3{\cdot}9H_2O$, $Sc(NO_3)_3{\cdot}9H_2O$ and citric acid with the mole ratio of citric acid to metal ions being 1:1. After drying, anode catalyst of $Sr_2FeMoO_{6-\delta}$ was introduced into the porous YSZ backbone (opposite to the LSM support layer) by impregnating the precursor solution as shown in section 2.1. Both the cathode and anode catalysts were calcined at 850 °C for 2 h in air. The impregnation/heat treating cycle was repeated to achieve the desired loadings of 30 wt. % both for cathode and anode. For the symmetrical anode cell, the tri-layer electrolyte supported scaffold (porous YSZ/YSZ/porous YSZ) was also manufactured by laminating three tape-casted green tapes and co-sintering at 1400 °C for 4 h. $Sr_2Fe_{1+x}Mo_{1-x}O_{6-\delta}$ catalysts were introduced into the porous YSZ layer in the same way as the single cell. The effective area of both the single and symmetrical cells were 0.35 cm^2.

Characterization

Phase structure of $Sr_2Fe_{1+x}Mo_{1-x}O_{6-\delta}$ powders were identified by the X-ray diffraction technique at room temperature using a Rigaku XRD diffractometer with monochromatic CuK_α radiation. For electrical conductivity measurement, $Sr_2Fe_{1+x}Mo_{1-x}O_{6-\delta}$ powders with different stoichiometric were pressed into rectangular bars and sintered at 1350 °C in air for 5 h, respectively. The relative density of the bars was 0.932, 0.958, 0.963, 0.982 for $Sr_2Fe_{1+x}Mo_{1-x}O_{6-\delta}$ (x = 0, 0.2, 0.35, 0.5), respectively. The electrical conductivity were measured by the DC four probe method in a temperature range from 550 to 800 °C, in 97% H_2–3% H_2O atmosphere. For electrochemical characterization of the SOFC, silver grids were coated onto the electrodes as the current collector with silver wires attached as the lead of current and voltage. The fuel cells were tested over the temperature range of 700–800 °C with the flow rate of the fuel (H_2 or C_3H_8) being 30 sccm while ambient air was used as the oxidant. Both the current–voltage curves and electrochemical impedance spectra were obtained using an IM6 Electrochemical Workstation (ZAHNER, Germany). The electrochemical impedance spectra were collected at open circuit over the frequency range from 0.01 Hz to 100 kHz with a 20 mV perturbation. Impedance measurements were also carried out on the symmetrical anode cells. The microstructure of the cells were examined by scanning electron microscopy (SEM) using a Hitachi S-4800-II microscope.

Results and discussion

Fig. 1 shows the XRD patterns of the synthesized $Sr_2Fe_{1+x}Mo_{1-x}O_{6-\delta}$ (x = 0, 0.2, 0.35, 0.5) powders calcined at 1100 °C for 5 h in air. As shown, pure phase $Sr_2Fe_{1.5}Mo_{0.5}O_{6-\delta}$ was obtained while a larger portion of $SrMoO_4$ second phase was detected in $Sr_2Fe_{1+x}Mo_{1-x}O_{6-\delta}$ (x = 0, 0.2, 0.35). The diffraction peaks of $SrMoO_4$ became more obvious when the content of Mo increased. This indicates that the ratio of Mo had a significant influence on the stability of the

Please cite this article in press as: Miao G, et al., $Sr_2Fe_{1+x}Mo_{1-x}O_{6-\delta}$ as anode material of cathode–supported solid oxide fuel cells, International Journal of Hydrogen Energy (2015), http://dx.doi.org/10.1016/j.ijhydene.2015.12.045

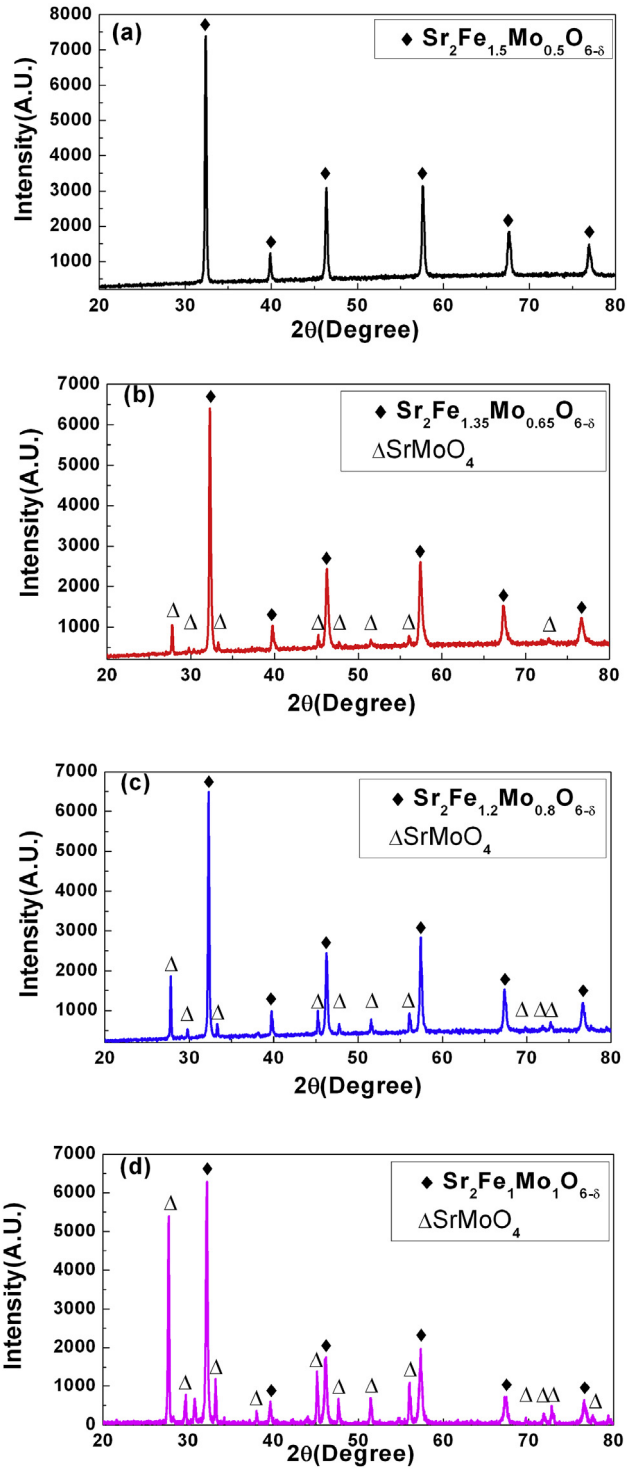

Fig. 1 – XRD patterns of the $Sr_2Fe_{1+x}Mo_{1-x}O_{6-\delta}$ powders calcined at 1100 °C for 5 h in air: (a) x = 0.5, (b) x = 0.35, (c) x = 0.2, (d) x = 0.

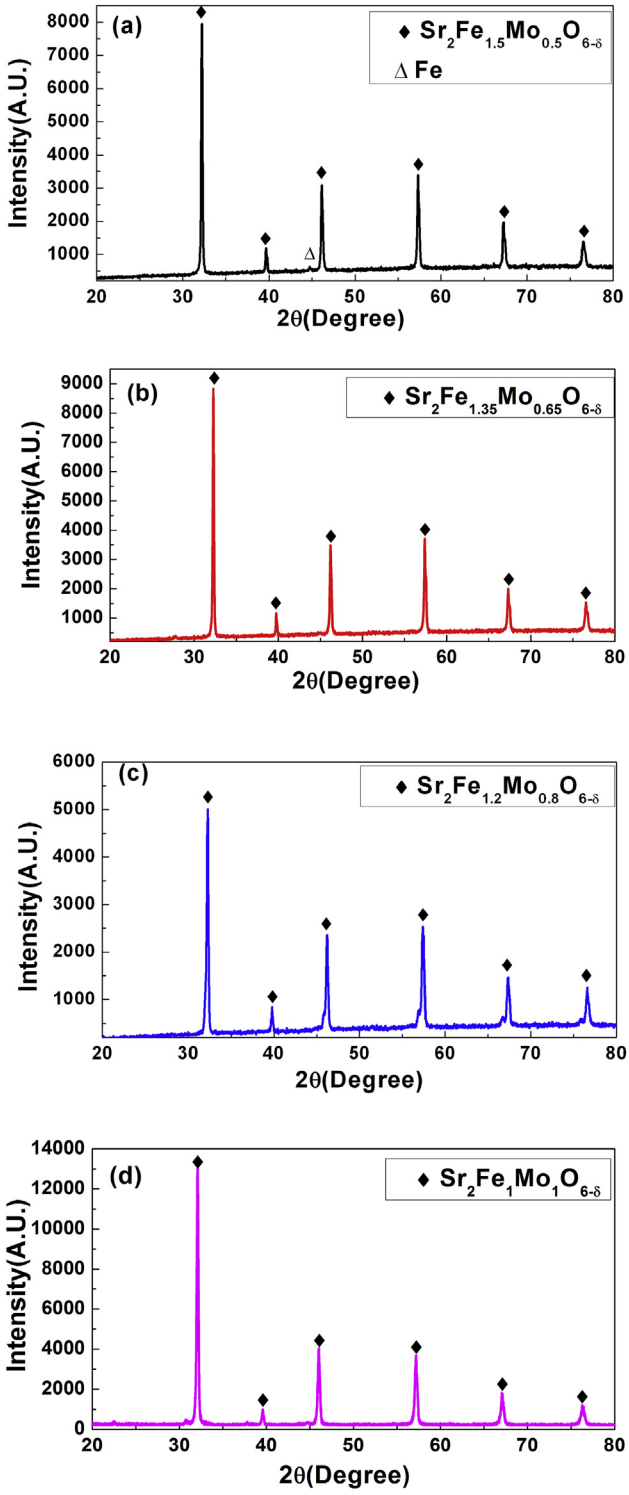

Fig. 2 – XRD patterns of $Sr_2Fe_{1+x}Mo_{1-x}O_{6-\delta}$ powders calcined at 1100 °C for 5 h in air followed by reducing at 800 °C for 10 h: (a) x = 0.5, (b) x = 0.35, (c) x = 0.2, (d) x = 0.

$Sr_2Fe_{1+x}Mo_{1-x}O_{6-\delta}$ in air. The experimental results are consistent with the previous study which showed that $Sr_2Fe_{1.5}Mo_{0.5}O_{6-\delta}$ could be synthesized in the oxidizing environment while $Sr_2FeMoO_{6-\delta}$ could only be synthesized in a reducing environment [22].

Powders obtained in air were then reduced in 97% H_2–3% H_2O at 800 °C for 10 h and the XRD patterns are shown in Fig. 2. A pure perovskite phase of $Sr_2Fe_{1+x}Mo_{1-x}O_{6-\delta}$ (x = 0, 0.2, 0.35) was formed after reduction. Meanwhile, minor amount of Fe

Please cite this article in press as: Miao G, et al., $Sr_2Fe_{1+x}Mo_{1-x}O_{6-\delta}$ as anode material of cathode–supported solid oxide fuel cells, International Journal of Hydrogen Energy (2015), http://dx.doi.org/10.1016/j.ijhydene.2015.12.045

precipitated from $Sr_2Fe_{1.5}Mo_{0.5}O_{6-\delta}$ was found. Wang et al. pointed out that irradiation-induced reducing atmospheres could cause the $Sr_2Fe_{1.5}Mo_{0.5}O_{6-\delta}$ to decompose to Fe and $Sr_4FeMoO_{8-\delta}$ [29]. However, more researches reported that $Sr_2Fe_{1.5}Mo_{0.5}O_{6-\delta}$ could be stable in reducing atmosphere without the precipitation of Fe [22,25,30]. Reasons of the conflicting conclusions are not known. To further study the influence of calcining duration on the precipitation of Fe, powder obtained above was reduced in 97% H_2–3% H_2O at 800 °C for another 10 h. However, $Sr_2Fe_{1+x}Mo_{1-x}O_{6-\delta}$ (x = 0, 0.2, 0.35) oxides were still stable in reducing atmosphere. The diffraction peak of precipitated Fe did not show obvious change and the reduced $Sr_2Fe_{1.5}Mo_{0.5}O_{6-\delta}$ oxide could retain the perovskite structure. It indicates that the amount of the metallic Fe is not increased and the reduced $Sr_2Fe_{1.5}Mo_{0.5}O_{6-\delta}$ oxide is stable after the extended exposure in reducing atmosphere.

The $Sr_2Fe_{1+x}Mo_{1-x}O_{6-\delta}$ anodes were prepared by impregnation in this work. Due to its reactivity and poor chemical capability with YSZ at high temperature [22,30], the calcining temperature of the impregnated anode was limited to only 850 °C, because a higher calcining temperature would result in the growth of impregnated particles and cause the performance degradation of cells' electrode [31,32]. To confirm the phase structure of the impregnated $Sr_2Fe_{1+x}Mo_{1-x}O_{6-\delta}$ anode applied in this study, XRD patterns of $Sr_2Fe_{1+x}Mo_{1-x}O_{6-\delta}$ (x = 0, 0.2, 0.35, 0.5) powders calcined at 850 °C for 2 h in air was measured. As shown in Fig. 3(a), all components showed the major impurity phases of $SrMoO_4$ and $SrFeO_{3-\delta}$ and no perovskite phase was detected. To simulate the cell operation environment, powders calcined at 850 °C in air were further reduced in 97% H_2–3% H_2O at 800 °C for 2 h. After the reducing process, pure perovskite phase was obtained for the components with Fe: Mo ratio being 1.2:0.8 and 1:1, while minor impurity of metallic Fe was detected for the components with Fe: Mo ratio being 1.35:0.65 and 1.5:0.5 (Fig. 3(b)).

Fig. 4(a) shows the temperature dependence of total electrical conductivities of $Sr_2Fe_{1+x}Mo_{1-x}O_{6-\delta}$ (x = 0, 0.2, 0.35, 0.5) in 97% H_2–3% H_2O. It can be seen that the electrical conductivity of $Sr_2Fe_{1+x}Mo_{1-x}O_{6-\delta}$ (x = 0, 0.2, 0.35, 0.5) is increased with the increasing content of Mo over the whole temperature range. $Sr_2FeMoO_{6-\delta}$ showed the highest electrical conductivity, e.g., 186.9 S cm^{-1} at 800 °C. Note that in the temperature range of 550–800 °C, $Sr_2FeMoO_{6-\delta}$ exhibited a metallic behavior while other compositions showed a semiconducting behavior [33], which means different stoichiometric $Sr_2Fe_{1+x}Mo_{1-x}O_{6-\delta}$ would follow different conduction mechanisms under different oxygen partial pressures. Fig. 4(b) shows the Arrhenius curves of the electrical conductivities and linear relationships can be observed for different samples.

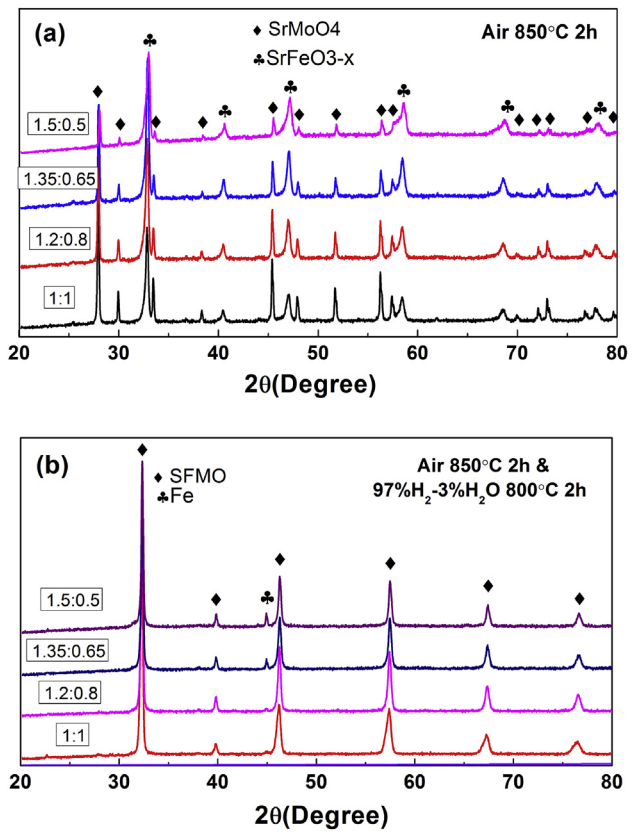

Fig. 3 – XRD patterns of $Sr_2Fe_{1+x}Mo_{1-x}O_{6-\delta}$ (x = 0.5, 0.35, 0.2, 0) powders: (a) Calcined at 850 °C for 2 h in air, (b) Calcined at 850 °C for 2 h in air followed by reducing in 97% H_2–3% H_2O at 800 °C for 2 h.

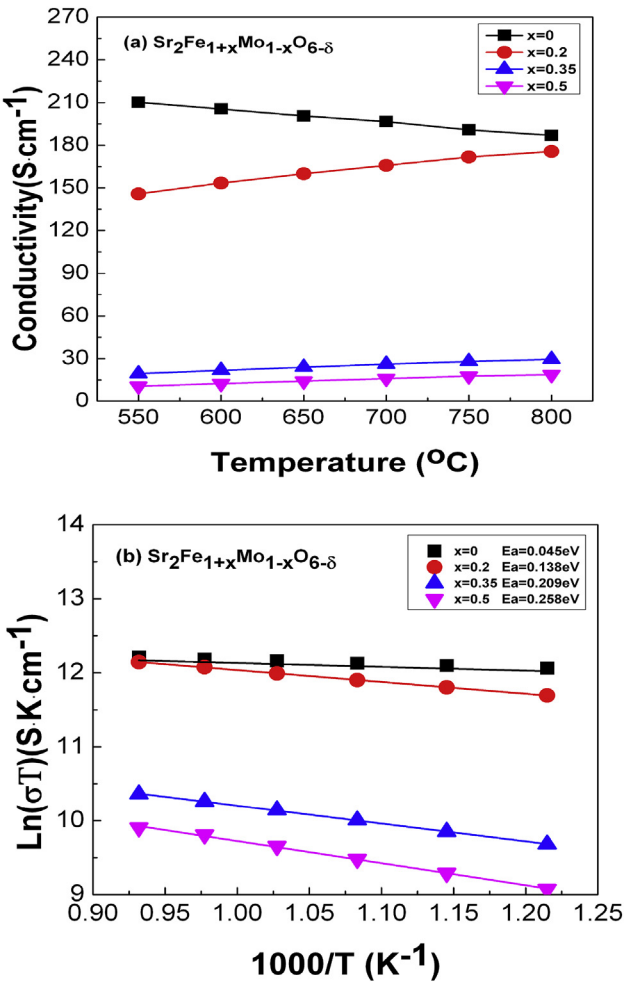

Fig. 4 – (a) Electrical conductivities and (b) Corresponding Arrhenius plots of the $Sr_2Fe_{1+x}Mo_{1-x}O_{6-\delta}$ (x = 0.5, 0.35, 0.2, 0) measured in 97% H_2–3% H_2O at 800 °C.

Please cite this article in press as: Miao G, et al., $Sr_2Fe_{1+x}Mo_{1-x}O_{6-\delta}$ as anode material of cathode–supported solid oxide fuel cells, International Journal of Hydrogen Energy (2015), http://dx.doi.org/10.1016/j.ijhydene.2015.12.045

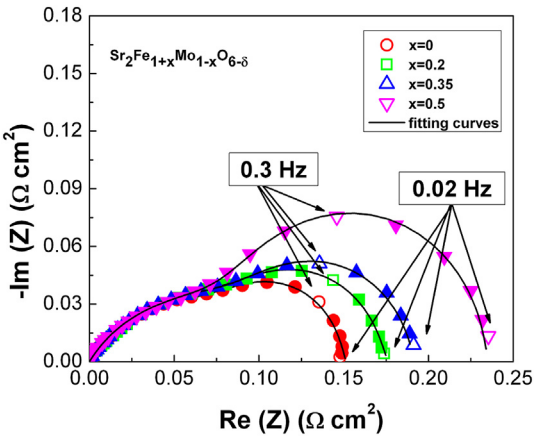

Fig. 5 – Electrochemical impedance spectra (EIS) of the impregnated $Sr_2Fe_{1+x}Mo_{1-x}O_{6-\delta}$ (x = 0.5, 0.35, 0.2, 0) symmetrical anode cells measured at 800 °C.

This means that the electrical conductivity behavior may be primarily determined by the small polaron conduction mechanism.

Fig. 5 shows the Nyquist plots of the impedance spectra data for symmetrical anode cells impregnated with different stoichiometric of $Sr_2Fe_{1+x}Mo_{1-x}O_{6-\delta}$ (x = 0, 0.2, 0.35, 0.5) measured in 97% H_2–3% H_2O at 800 °C. The ohmic response of the electrolyte and electrodes were removed while the resistances were divided by 2 to account for the contributions of two symmetrical electrodes. As shown, the polarization result was 0.235, 0.193, 0.176 and 0.152 Ω cm² for the component with x = 0.5, 0.35, 0.2 and 0, respectively. The polarization resistance of cells' anode decreased with the increasing amount of Mo, which means that the content of Mo has a serious effect on the performance of the cell. All the spectra consist of two

Table 1 – Fitted impedance results of the impregnated $Sr_2Fe_{1+x}Mo_{1-x}O_{6-\delta}$ (x = 0, 0.2, 0.35, 0.5) symmetrical anode cells.

x	R_{HF} (Ω cm²)	R_{LF} (Ω cm²)
0	0.10	0.054
0.2	0.11	0.066
0.35	0.11	0.084
0.5	0.10	0.13

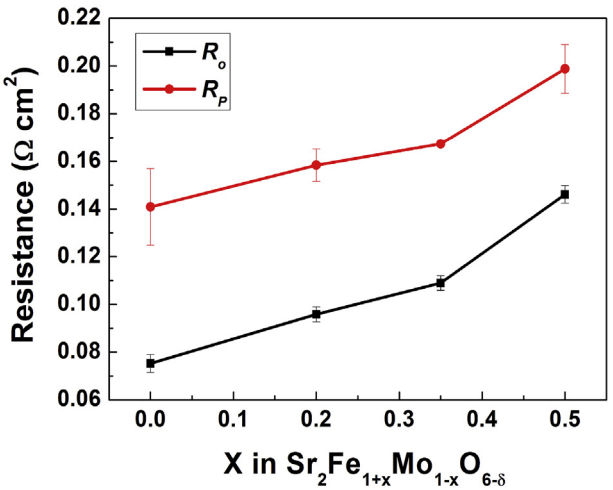

Fig. 6 – Ohmic and polarization resistances of the impregnated $Sr_2Fe_{1+x}Mo_{1-x}O_{6-\delta}$ (x = 0.5, 0.35, 0.2, 0) symmetrical anode cells measured at 800 °C.

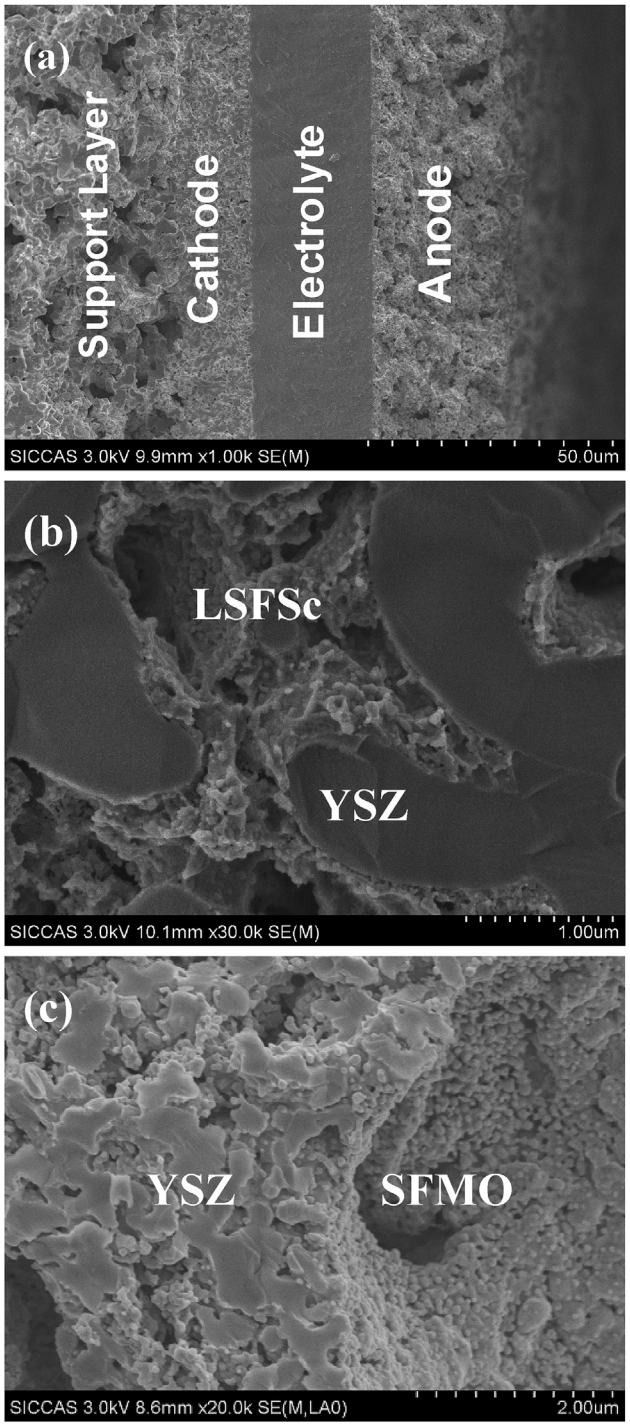

Fig. 7 – Cross-section SEM images of: (a) The single cell, (b) The LSFSc impregnated YSZ cathode, (c) The $Sr_2FeMoO_{6-\delta}$ impregnated YSZ anode.

Please cite this article in press as: Miao G, et al., $Sr_2Fe_{1+x}Mo_{1-x}O_{6-\delta}$ as anode material of cathode–supported solid oxide fuel cells, International Journal of Hydrogen Energy (2015), http://dx.doi.org/10.1016/j.ijhydene.2015.12.045

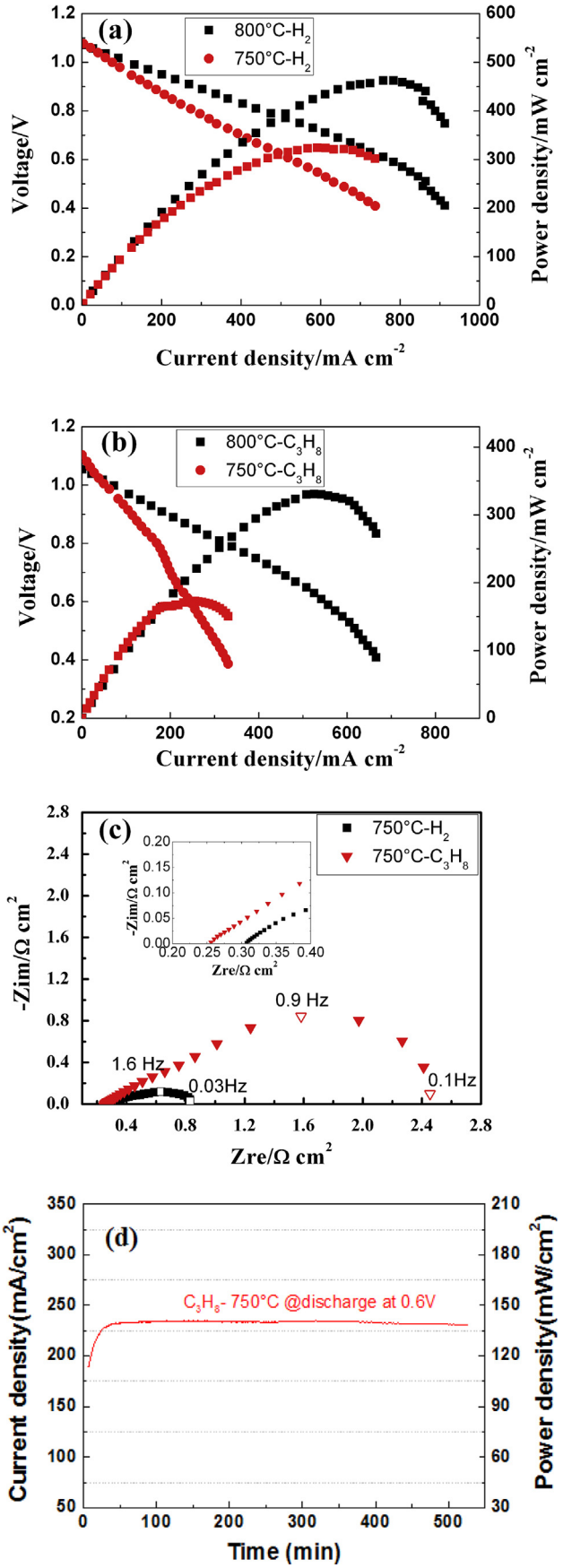

Fig. 8 – Current-voltage characteristics of the single cell measured in (a) humidified H_2 and (b) humidified C_3H_8 at 750 and 800 °C. (c) is the electrochemical impedance of the single cell measured at 750 °C in wet H_2 and C_3H_8, respectively. (d) Stability of a single cell operated in C_3H_8 at 0.6 V and 750 °C.

semicircles which can be separated according to the frequency. The impedance spectra were fitted via an equivalent circuit with a configuration of R_{ohm} (R_{HF}-CPE_{HF}) (R_{LF}-CPE_{LF}) [34]. R_{ohm} is the overall ohmic resistance including electrolyte resistance and electrode ohmic resistance. CPE_{HF} and CPE_{LF} are constant phase elements while R_{HF} and R_{LF} refer to the high and low frequency resistances, corresponding to different chemical reaction processes, respectively. The fitting results are shown in Table 1, which indicates the effect of Mo content on the high and low frequency resistances (R_{HF} and R_{LF}). Major difference in impedance spectra among these components is in the lower frequency part. Since the lower frequency arc is usually associated with the surface kinetics, impedance spectra difference shown in Fig. 5 may refer to the difference in oxygen vacancy formation processes on the surface of $Sr_2Fe_{1+x}Mo_{1-x}O_{6-\delta}$. It was reported that with the increasing of Mo concentration on the exposed layer, the oxygen vacancy formation energy will decrease and anodic reaction activity will increase [18].

Ohmic and polarization resistances of the cells with impregnated $Sr_2Fe_{1+x}Mo_{1-x}O_{6-\delta}$ anode cells measured at 800 °C in 97% H_2–3% H_2O are compared in Fig. 6. It can be seen that both the ohmic and polarization resistance decrease with the increasing content of Mo. Since the electrical conductivity of $Sr_2Fe_{1+x}Mo_{1-x}O_{6-\delta}$ increases with the increasing content of Mo, while the electrons generated in the anode reaction is transferred by the $Sr_2Fe_{1+x}Mo_{1-x}O_{6-\delta}$ particles connecting with each other, there is no wound that the ohmic resistance would decrease with increasing conductivity of the particles.

Fig. 7(a) shows the cross-sectional microstructure of the cathode-supported fuel cell. The single cell contained a dense electrolyte layer sandwiched between two porous YSZ layers and supported by the thick porous LSM backbone. This structure design is beneficial for achieving intimate contact between different layers, producing a dense electrolyte on the porous structure and providing sufficient porosity for the gas transport. The YSZ electrolyte layer was fully dense with a thickness of 24 μm. Due to the phase stability in anode atmosphere and low polarization resistance of $Sr_2FeMoO_{6-\delta}$, this component was selected as the anode in the single cell. As shown in Fig. 7(b) and (c), the nano-scaled particles of LSFSc and $Sr_2FeMoO_{6-\delta}$ catalysts with particle sizes of 50–100 nm are internal-connected and well coated onto the inner surface of the porous YSZ backbones.

Electrochemical performances of the single fuel cell with humidified hydrogen fuel and air oxidant measured at 750 and 800 °C are shown in Fig. 8(a). The maximum powder density (MPD) was 324 and 462 mW cm^{-2} at 750 and 800 °C, respectively. This result is comparable to the result obtained in a $La_{0.8}Sr_{0.2}Ga_{0.83}Mg_{0.17}O_3$ (LSGM) electrolyte-supported fuel cell using $Sr_2Fe_{1.5}Mo_{0.5}O_{6-\delta}$ as the anode [24]. The different cell performances may be attributed to the different cell structures and electrode materials. Fig. 8(b) shows the performance of the cell with C_3H_8 as fuel, the peak power density of 173 and

Please cite this article in press as: Miao G, et al., $Sr_2Fe_{1+x}Mo_{1-x}O_{6-\delta}$ as anode material of cathode–supported solid oxide fuel cells, International Journal of Hydrogen Energy (2015), http://dx.doi.org/10.1016/j.ijhydene.2015.12.045

331 mW cm^{-2} was obtained at 750 and 800 °C, respectively. Electrochemical impedance spectra (EIS) of the single cells measured at open circuit and 750 °C using wet hydrogen and propane as the fuel are shown in Fig. 8(c). The ohmic resistance corresponds to the high-frequency real-axis intercept and the electrode polarization resistance is taken by subtracting the ohmic resistance (high-frequency intercept at real-axis) from the total resistance (low-frequency intercept at real-axis). The ohmic resistance was 0.31 and 0.25 Ω cm^2 for cell feeding with hydrogen and propane, respectively. In contrast, the polarization resistance was 0.52 and 2.11 Ω cm^2, respectively. Obviously, the impedance spectra difference of the cell using H_2 and C_3H_8 as fuel is mainly from the polarization loss, especially at the low-frequency. This difference may be caused by the variation of the activation and diffusion processes in the anode.

Fig. 8(d) shows the stability of the single cell operated in propane at 750 °C and 0.6 V. No obvious degradation was found during the 530 min test. This indicates that $Sr_2FeMoO_{6-\delta}$ impregnated porous YSZ anode showed good resistance against the carbon deposition. An extended measurement is needed to further study the cell stability in propane.

Conclusions

Phase stability of the $Sr_2Fe_{1+x}Mo_{1-x}O_{6-\delta}$ (x = 0, 0.2, 0.35, 0.5) powder was investigated in this study. After calcining at 1100 °C in air, pure $Sr_2Fe_{1.5}Mo_{0.5}O_{6-\delta}$ phase could be obtained while a large portion of $SrMoO_4$ second phase was detected in $Sr_2Fe_{1+x}Mo_{1-x}O_{6-\delta}$ (x = 0, 0.2, 0.35). Pure phase for $Sr_2Fe_{1+x}Mo_{1-x}O_{6-\delta}$ (x = 0, 0.2, 0.35) were obtained after reducing the above powders in 97% H_2–3% H_2O at 800 °C for 10 h, while minor amount of Fe was precipitated from the $Sr_2Fe_{1.5}Mo_{0.5}O_{6-\delta}$. The extending reducing time made no obvious influence on the phase structure. Compared to other components, $Sr_2FeMoO_{6-\delta}$ impregnated YSZ anode showed the lowest polarization resistance, e.g. 0.152 Ω cm^2 at 800 °C. Cathode-supported SOFC employing the $Sr_2FeMoO_{6-\delta}$ impregnated YSZ anode reached the maximum power density of 462 and 331 mW cm^{-2} at 800 °C, using H_2 and C_3H_8 as the fuel, respectively. Durability test of the fuel cell in C_3H_8 showed a relatively stable performance.

Acknowledgment

We gratefully acknowledge the financial support from the Science and Technology Commission of Shanghai Municipality (No. 12160706500) and National Natural Science Foundation of China (No. 51172266).

REFERENCES

[1] Atkinson A, Barnett S, Gorte RJ, Irvine JTS, McEvoy AJ, Mogensen M, et al. Advanced anodes for high-temperature fuel cells. Nat Mater 2004;3:17–27.
[2] Murray EP, Tsai T, Barnett SA. A direct-methane fuel cell with a ceria-based anode. Nature 1999;400:649–51.
[3] Park SD, Vohs JM, Gorte RJ. Direct oxidation of hydrocarbons in a solid-oxide fuel cell. Nature 2000;404:265–7.
[4] Gorte RJ, Kim H, Vohs JM. Novel SOFC anodes for the direct electrochemical oxidation of hydrocarbon. J Power Sources 2002;106:10–5.
[5] Yamazaki O, Tomishige K, Fujimoto K. Development of highly stable nickel catalyst for methane steam reaction under low steam to carbon ratio. Appl Catal A Gen 1996;136:49–56.
[6] Sun C, Stimming U. Recent anode advances in solid oxide fuel cells. J Power Sources 2007;171:247–60.
[7] Cowin PI, Petit CTG, Lan R, Irvine JTS, Tao S. Recent progress in the development of anode materials for solid oxide fuel cells. Adv Energy Mater 2011;1:314–32.
[8] Finnerty CM, Coe NJ, Cunningham RH, Ormerod RM. Carbon formation on and deactivation of nickel-based/zirconia anodes in solid oxide fuel cells running on methane. Catal Today 1998;46:137–45.
[9] Zhou X, Yan N, Chuang KT, Luo J. Progress in La-doped $SrTiO_3$ (LST)-based anode materials for solid oxide fuel cells. RSC Adv 2014;4:118–31.
[10] Tao SW, Irvine JTS. A redox-stable efficient anode for solid-oxide fuel cells. Nat Mater 2003;2:320–3.
[11] Tao SW, Irvine JTS. Catalytic properties of the perovskite oxide $La_{0.75}Sr_{0.25}Cr_{0.5}Fe_{0.5}O_{3-\delta}$in relation to its potential as a solid oxide fuel cell anode material. Chem Mater 2004;16:4116–21.
[12] Huang YH, Dass RI, Xing ZL, Goodenough JB. Double perovskites as anode materials for solid-oxide fuel cells. Science 2006;312:254–7.
[13] Huang YH, Dass RI, Denyszyn JC, Goodenough JB. Synthesis and characterization of $Sr_2MgMoO_{6-\delta}$ an anode material for the solid oxide fuel cell. J Electrochem Soc 2006;153:A1266–72.
[14] Huang Y-H, Liang G, Croft M, Lehtimaki M, Karppinen M, Goodenought JB. Double-perovskite anode materials Sr_2MMoO_6 (M = Co, Ni) for solid oxide fuel cells. Chem Mater 2009;21:2319–26.
[15] Xiao G, Liu Q, Zhao F, Zhang L, Xia C, Chen F. $Sr_2Fe_{1.5}Mo_{0.5}O_6$ as cathodes for intermediate-temperature solid oxide fuel cells with $La_{0.8}Sr_{0.2}Ga_{0.87}Mg_{0.13}O_3$ electrolyte. J Electrochem Soc 2011;158:B455–60.
[16] Dai N, Lou Z, Wang Z, Liu X, Yan Y, Qiao J, et al. Synthesis and electrochemical characterization of $Sr_2Fe_{1.5}Mo_{0.5}O_6$-$Sm_{0.2}Ce_{0.8}O_{1.9}$ composite cathode for intermediate-temperature solid oxide fuel cells. J Power Sources 2013;243:766–72.
[17] Zhou Y, Meng X, Ye X, Li J, Wang S, Zhan Z. Metal-supported solid oxide fuel cells with impregnated $SrFe_{0.75}Mo_{0.25}O_3$ cathodes. J Power Sources 2014;247:556–61.
[18] Suthirakun S, Arnmal SC, Munoz-Garcia AB, Xiao G, Chen F, zur Loye H-C, et al. Theoretical investigation of H_2 oxidation on the $Sr_2Fe_{1.5}Mo_{0.5}O_6$ (001) perovskite surface under anodic solid oxide fuel cell conditions. J Am Chem Soc 2014;136:8374–86.
[19] Hou M, Sun W, Li P, Feng J, Yang G, Qiao J, et al. Investigation into the effect of molybdenum-site substitution on the performance of $Sr_2Fe_{1.5}Mo_{0.5}O_{6-\delta}$ for intermediate temperature solid oxide fuel cells. J Power Sources 2014;272:759–65.
[20] Walker E, Ammal SC, Suthirakun S, Chen F, Terejanu GA, Heyden A. Mechanism of sulfur poisoning of $Sr_2Fe_{1.5}Mo_{0.5}O_{6-\delta}$ perovskite anode under solid oxide fuel cell conditions. J Phys Chem C 2014;118:23545–52.
[21] Munoz-Garcia AB, Bugaris DE, Pavone M, Hodges JP, Huq A, Chen F, et al. Unveiling structure-property relationships in

$Sr_2Fe_{1.5}Mo_{0.5}O_{6-\delta}$, an electrode material for symmetric solid oxide fuel cells. J Am Chem Soc 2012;134:6826–33.

[22] Liu Q, Dong X, Xiao G, Zhao F, Chen F. A novel electrode material for symmetrical SOFCs. Adv Mater 2010;22:5478–82.

[23] Sun C, Hui R, Roller J. Cathode materials for solid oxide fuel cells: a review. J Solid State Electrochem 2010;14:1125–44.

[24] Li H, Tian Y, Wang Z, Qie F, Li Y. An all perovskite direct methanol solid oxide fuel cell with high resistance to carbon formation at the anode. RSC Adv 2012;2:3857–63.

[25] Wang Z, Tian Y, Li Y. Direct CH_4 fuel cell using Sr_2FeMoO_6 as an anode material. J Power Sources 2011;196:6104–9.

[26] Xiao G, Liu Q, Nuansaeng S, Chen F. $Sr_2Fe_{1+x}Mo_{1-x}O_{6-\delta}$ as anode materials for solid oxide fuel cells. Ionic Mix Conducting Ceram 8 2012;45:355–62.

[27] Yuan C, Liu Y, Zhou Y, Zhan Z, Wang S. Fabrication and characterization of a cathode-support solid oxide fuel cell by tape casting and lamination. Int J Hydrogen Energy 2013;38:16584–9.

[28] Yuan C, Luo T, Li J, Meng X, Qian J, Ye X, et al. Infiltrated porous YSZ as a cathode active layer for cathode-supported solid oxide fuel cells. Electrochem Commun 2014;46:40–3.

[29] Wang S, Tang M, Brinkman KS, Chen F. Ion-irradiation induced reduction in $Sr_2Fe_{1.5}Mo_{0.5}O_{6-\delta}$ perovskite. Nucl Instrum Methods Phys Res Sect B Beam Interact Mater Atoms 2014;326:298–302.

[30] dos Santos-Gomez L, Leon-Reina L, Porras-Vazquez JM, Losilla ER, Marrero-Lopez D. Chemical stability and compatibility of double perovskite anode materials for SOFCs. Solid State Ionics 2013;239:1–7.

[31] Zhou Y, Han D, Yuan C, Liu M, Chen T, Wang S, et al. Infiltrated $SmBa_{0.5}Sr_{0.5}Co_2O_{5+\delta}$ cathodes for metal-supported solid oxide fuel cells. Electrochimica Acta 2014;149:231–6.

[32] Meng X, Han D, Wu H, Li J, Zhan Z. Characterization of $SrFe_{0.75}Mo_{0.25}O_{3-\delta}$-$La_{0.9}Sr_{0.1}Ga_{0.8}Mg_{0.2}O_{3-\delta}$ composite cathodes prepared by infiltration. J Power Sources 2014;246:906–11.

[33] Zhang L, Zhou Q, He Q, He T. Double-perovskites A(2) FeMoO(6-delta) (A = Ca, Sr, Ba) as anodes for solid oxide fuel cells. J Power Sources 2010;195:6356–66.

[34] Zhou W, Ran R, Shao Z, Zhuang W, Jia J, Gu H, et al. Barium- and strontium-enriched $(Ba_{(0.5)}Sr_{(0.5)})_{(1+x)}Co_{(0.8)}Fe_{(0.2)}O_{(3-\delta)}$ oxides as high-performance cathodes for intermediate-temperature solid-oxide fuel cells. Acta Mater 2008;56:2687–98.

Please cite this article in press as: Miao G, et al., $Sr_2Fe_{1+x}Mo_{1-x}O_{6-\delta}$ as anode material of cathode–supported solid oxide fuel cells, International Journal of Hydrogen Energy (2015), http://dx.doi.org/10.1016/j.ijhydene.2015.12.045